

New boron-based coumarin fluorophores for bioimaging applications[†]

 Anita Marfavi^{A,B}, Jia Hao Yeo^A , Kathryn G. Leslie^A, Elizabeth J. New^{A,B,C}  and Louis M. Rendina^{A,B,*} 

For full list of author affiliations and declarations see end of paper

***Correspondence to:**

 Louis M. Rendina
 School of Chemistry, The University of
 Sydney, Sydney, NSW 2006, Australia
 Email: louis.rendina@sydney.edu.au
Handling Editor:

George Koutsantonis

Received: 3 December 2021

Accepted: 7 February 2022

Published: 29 March 2022

Cite this:

 Marfavi A et al. (2022)
Australian Journal of Chemistry
75(8 & 9), 716–724. doi:[10.1071/CH21320](https://doi.org/10.1071/CH21320)

 © 2022 The Author(s) (or their
 employer(s)). Published by
 CSIRO Publishing.

 This is an open access article distributed
 under the Creative Commons Attribution-
 NonCommercial-NoDerivatives 4.0
 International License ([CC BY-NC-ND](https://creativecommons.org/licenses/by-nc-nd/4.0/))

OPEN ACCESS

ABSTRACT

The synthesis and characterisation of five new boron-based coumarin fluorophores are reported, with key structural variations involving the linker at the C3-position (hydrazone or imine) of the 7-(diethylamino)-coumarin (**7DEAC**) core and the terminal boron moiety (i.e. boronic acid or *closo*-1,2-carborane). All the coumarin derivatives were found to display significant bathochromic shifts relative to the parent **7DEAC**, with conjugate **ICCb** displaying the greatest overall shift. Confocal microscopy studies with A549 lung cancer cells showed clear differences in the observed intra-cellular distributions of the fluorophores. The polar boronic acid species (**HCoBA**, **HCmBA** and **HCpBA**) were found to localise in the endoplasmic reticulum. In contrast, the lipophilic *closo*-1,2-carborane derivatives (**HCCb** and **ICCb**) were found to localise within lipid droplets (LDs), showcasing the future potential for these probes to be utilised as stains for LD observations by means of confocal microscopy.

Keywords: bioimaging, boron, coumarin, endoplasmic reticulum, fluorescence microscopy, fluorescent probes, fluorophore, intramolecular charge transfer, lipid droplets, near-infrared, Nile Red.

Introduction

Understanding the nature of complex biological events occurring in normal cellular physiology and pathology is fundamental to developing novel strategies for disease prevention, diagnosis and treatment. Fluorescence imaging, including confocal microscopy, has emerged as a landmark platform providing detailed cellular analysis with high sensitivity and selectivity.^[1] These applications have also extended across an array of biomedical platforms, including non-invasive image guided surgery,^[2,3] contrast agents, detection of tumours, tracking drug metabolism, monitoring biological processes (for example, thrombotic activity)^[4] and for the detection of many types of metal ions.^[5] In biological imaging, significant bathochromic shifts towards the near-infrared (NIR) region enables greater tissue penetration, reduced light scattering and minimal cellular autofluorescence.^[6]

Significant drawbacks undermining existing organic biological probes include low aqueous solubility and small Stokes shifts. Coumarins are an important class of fluorophores that exhibit exceptional photophysical properties, with large Stokes shifts, high quantum yields, small molecular weights and good water solubility. Although their emission is relatively blue-shifted (410–470 nm), their ease of functionalisation can be exploited such that the photophysical properties may be improved to generate biologically useful fluorophores.^[7,8] The most fundamental coumarin design strategy is to incorporate an electron-donating group at the 7-position (C7). This results in a ‘push–pull’ mechanism, contributing to an intramolecular charge transfer (ICT) during excitation via photon absorption. The ICT process is aided by the addition of electron-withdrawing or -donating groups (EWG or EDG, respectively) at the 3- or 4-positions (C3/C4) to red-shift the fluorescence spectra via resonance and inductive effects.^[9]

[†]Dedicated to Prof. Glen B. Deacon, on the occasion of his 85th birthday and in recognition of his many outstanding contributions to organometallic chemistry.

In particular, the incorporation of *N*-acylhydrazone derivatives (Schiff bases) has been well documented in coumarin derivatives that can detect metal ions.^[7] In addition, an extended unsaturated π -conjugated bridge at C3 has led to extensive bathochromic shifts and more pronounced molar extinction coefficients.^[10,11] Increasing the electron-donor strength at C7 (e.g. $-\text{N}(\text{C}_2\text{H}_5)_2 > -\text{OH} > -\text{OCH}_3$) also increases the red-shift in the fluorescence spectra.

Electron-deficient boron moieties, including boronic acids and *C*-substituted *closo*-1,2-carboranes, which can act as bioisosteres of phenyl rings, can be utilised as terminal EWGs to facilitate the ICT process and enhance the bathochromic shift of new fluorescent probes.^[12,13] Boronic acids have been incorporated into fluorophores for the selective detection of metal ions for medicinal and environmental research.^[14] Remarkably, carboranes have shown utility in the design of fluorescent probes with enhanced pharmacokinetics, stability and bathochromic shifts for applications in biological imaging and sensing.^[15,16] We have previously demonstrated the lipophilic nature of *closo*-carboranes in the development of a carborane-containing coumarin which localises in cellular lipid droplets, as an alternative to the lipid-staining dye Nile Red.^[13] The versatility of carboranes as luminescent sensors for fluoride anions has been reported,^[17] with a donor-acceptor molecule comprised of an *ortho*-carborane unit and a bulky, tri-coordinate organoboron compound, a dimesitylboryl group (BMe_2).

To the best of our knowledge, there are no reports providing a direct comparison of the intracellular distributions between various boron functional groups in coumarin fluorescent probes. Herein we report the synthesis and characterisation of new boron-based coumarins conjugated via hydrazone or imine linkers, with extensive consideration to structure-photophysical property relationships. Cell uptake and biodistribution of selected boronated fluorophores were also investigated to assess their potential as new biological stains for confocal microscopy.

Results and discussion

Probe design and synthesis

The main synthetic approach in the design of these novel coumarin fluorophores involved structural modifications of the parent 7-(diethylamino)-coumarin (**7DEAC**) scaffold. In this study, two main strategies were adopted: (a) the addition of an EWG at C3 (hydrazone linker) or (b) extension of the π -conjugation at C3 (imino linker) using a 3-formylcoumarin precursor (Fig. 1). These strategies were used in combination with the 7-diethylamino EDG at C7 of the coumarin framework and the addition of terminal boronic acid or *closo*-1,2-carborane moieties, to enhance the ICT process, increase the Stokes shift and ultimately generate a bathochromic shift in the excitation and emission

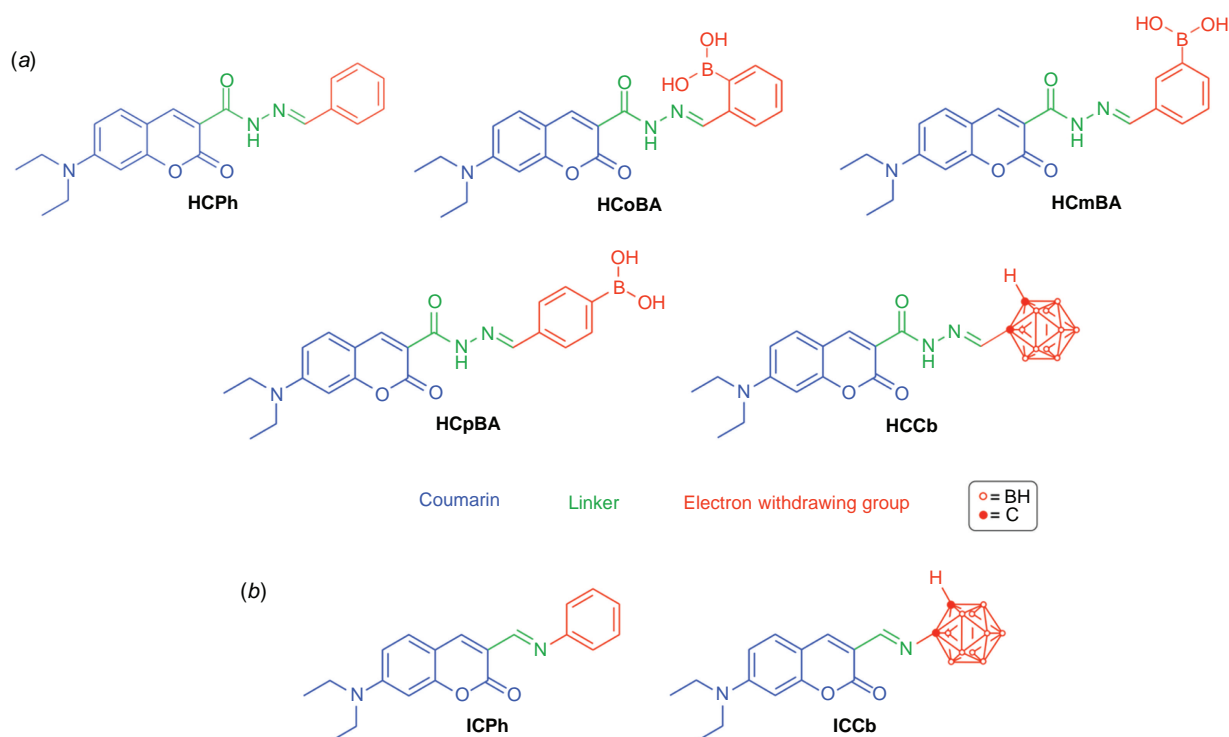
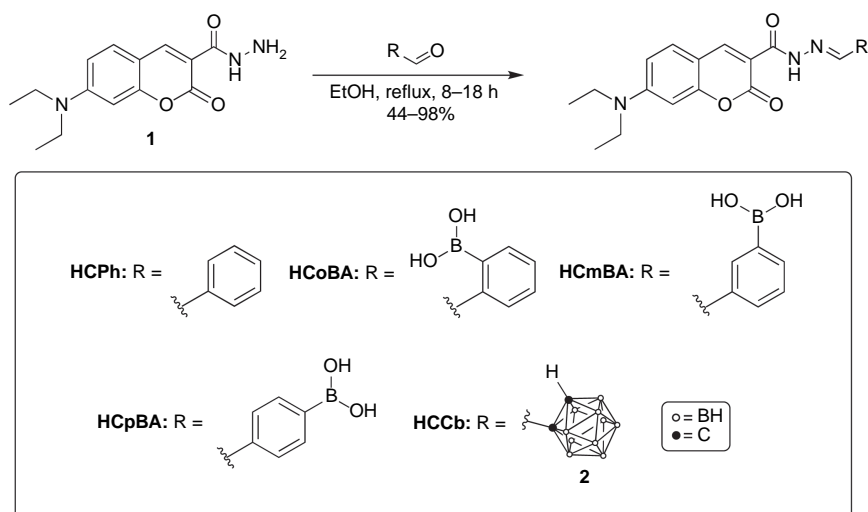


Fig. 1. Coumarin fluorophores prepared in this work: (a) hydrazone-coumarin derivatives and (b) imino-coumarin conjugates. Coumarin scaffold: blue, linker: green and electron-withdrawing group (EWG): red.



Scheme 1. Synthesis of hydrazone-coumarin derivatives (**HCPH**, **HCoBA**, **HCmBA**, **HCpBA** and **HCCb**).

maxima. Cumulatively, these structural modifications afforded four new hydrazone-coumarin conjugates and one imino-coumarin derivative, with two phenyl-containing analogues also included for comparison.

Synthesis of the hydrazone-coumarins initially involved a Knoevenagel condensation reaction between 4-(diethylamino)salicylaldehyde and diethyl malonate in the presence of a suitable base (piperidine).^[18] The coumarin ester was readily converted into the carbohydrazone by a nucleophilic substitution reaction with hydrazine hydrate, according to the literature procedure.^[19] Hydrazone formation occurred by means of a nucleophilic addition reaction between the carbohydrazone coumarin and formyl-functionalised benzaldehydes, such as 2, 3 or 4-formylphenylboronic acids, affording **HCPH**, **HCoBA**, **HCmBA** and **HCpBA**, respectively (Scheme 1). Mono-substituted formyl-*ortho*-carborane was prepared by means of a nucleophilic substitution with *n*-BuLi, proceeded by electrophilic functionalisation with methyl formate, and subsequent hydrazone formation (**HCCb**, Scheme 1) was achieved as above.

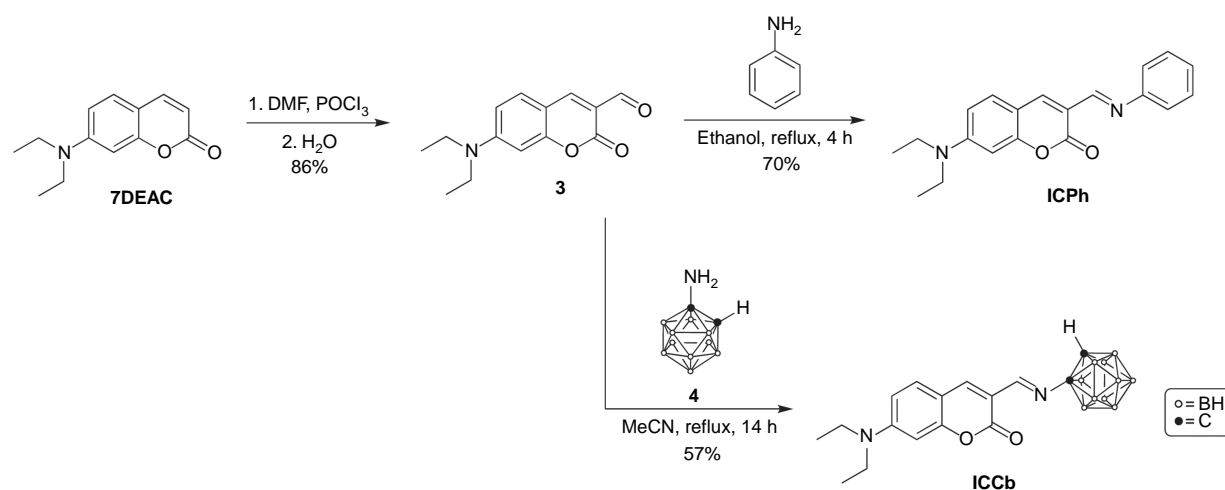
The first step in the synthesis of the imino-coumarin analogues was the formation of the parent **7DEAC**, once again using a Knoevenagel condensation (see above), followed by acid reflux and decarboxylation by the addition of NaOH. The formation of 3-formylcoumarin (**3**) occurred in the following step, whereby the C3-position of the coumarin backbone is subjected to an electrophilic attack by a Vilsmeier–Haack reagent. Imine formation then occurred by means of an electrophilic attack between 3-formylcoumarin and either aniline or 1-amino-*ortho*-carborane to give **ICPh** and **ICCb** (Scheme 2).

Fluorescence studies

Preliminary fluorescence studies were performed to investigate the impact of substitution (with EWGs and π -conjugated bridges) at the C3-position of the parent **7DEAC**.

Coumarin fluorescence involves an ICT-induced mechanism, and perturbations in the ICT process can alter fluorescence properties. Evidently, the coumarins containing a hydrazone linker (**HCPH**, **HCoBA**, **HCmBA**, **HCpBA** and **HCCb**) exhibited similar excitation and emission maxima, which are both red-shifted relative to the parent coumarin (Table 1). As expected, due to the absence of a π -conjugated bridge, the hydrazone moiety does not appear to extensively enhance the bathochromic shift. The nature of the terminal EWGs in the hydrazone-coumarins also appears to have a minimal effect on their photophysical properties.

Conversely, a trend was established regarding the impact of π -conjugation and a comparison of phenyl and *closo*-1,2-carborane moieties, as observed for compounds **ICPh** and **ICCb**. The inclusion of a π -conjugated bridge with a terminal EWG leads to a significant red-shift in both the observed excitation and emission maxima. As expected, *closo*-1,2-carborane is more electron-withdrawing than a phenyl substituent, and this leads to a larger bathochromic shift (ca. λ_{em} increase by 45 nm (**ICCb**) and 30 nm (**ICPh**), as compared to **7DEAC**). **ICCb** exhibited the most red-shifted emission maximum at 505 nm. Interestingly, the hydrazone-based coumarin derivatives showed higher quantum yields than the iminocoumarins, with the *para*-phenylboronic acid species **HCpBA** displaying the highest quantum yield (0.32). However, when compared to the parent, non-boronated **7DEAC**, the quantum yields were found to be significantly reduced. In the imino-coumarin species (**ICPh** and **ICCb**) the *ortho*-1,2-carborane derivative displayed a ca. 4-fold increase in quantum yield compared to its phenyl counterpart. The variability in the quantum yields across both species suggests that both the linker and terminal EWG are crucial determinants in this particular photophysical property. Furthermore, the relative overall brightness was greatest in the hydrazone-coumarin derivatives, with **HCpBA** displaying the highest value.



Scheme 2. Synthesis of imino-coumarin derivatives (**ICPh** and **ICCb**).

Table 1. Spectroscopic properties of coumarin derivatives in ethanol.

Fluorophore	λ_{ex} (nm)	λ_{em} (nm)	Φ_f	ϵ (M ⁻¹ cm ⁻¹)	Brightness ^A (M ⁻¹ cm ⁻¹)
7DEAC	378	459	0.79	–	–
HCPH	435	475	0.29	2.5×10^4	7.3×10^3
HCoBA	433	475	0.17	4.3×10^4	7.3×10^3
HCmBA	433	475	0.26	5.5×10^4	1.4×10^4
HCpBA	435	475	0.32	5.7×10^4	1.8×10^4
HCCb	425	478	0.05	1.1×10^4	5.5×10^2
ICPh	448	488	0.04	4.2×10^4	1.7×10^3
ICCb	465	505	0.15	1.0×10^4	1.5×10^3

^ABrightness (B) was calculated using the following equation: $B = \Phi_f \epsilon$.

Density functional theory calculations

Density functional theory (DFT) calculations (B3LYP/6-31G**) were performed for all the new coumarin derivatives prepared in this work (Table 2, see below). The results showed the π -conjugated imino-coumarin derivatives (**ICPh** and **ICCb**) exhibited the lowest HOMO–LUMO energy gap (ΔE). As expected, the imino linker at C3 significantly improves the red-shift in the spectroscopic profiles, by lowering the energy of the electronic transitions thereby generating longer emission wavelengths. Furthermore, while an EWG such as hydrazone can enhance the ICT process, a π -conjugated bridge provides a more substantial contribution to the photophysical properties. A similar trend was observed between the calculated wavelengths (λ , Table 2) and the excitation wavelengths measured for each coumarin probe (Table 1), whereby the imino-coumarin derivatives (**ICPh** and **ICCb**) displayed a greater bathochromic shift.

Confocal microscopy

One key aim of this work was to develop novel probes for bioimaging applications. To assess whether the compounds

are suitable for imaging studies, human alveolar basal epithelial (A549) cells were investigated. A549 cells were incubated with the coumarin fluorophores (10 μ M, 20 min) and imaged using a confocal microscope (Fig. 2, Supplementary Fig. S1).

Preliminary imaging studies revealed variations in sub-cellular distribution across the set of compounds, according to the polarity of the boron or phenyl moiety (boronic acid > phenyl > *closo*-1,2-carborane, Fig. 2). Coumarins bearing hydrophobic moieties (i.e. *closo*-1,2-carborane) exhibited punctate fluorescent staining, consistent with lipid droplets, as previously observed (Fig. 2c).^[13] Despite the bioisosteric relationship between phenyl and *closo*-1,2-carborane, the cytoplasmic and weakly diffusive fluorescence from the phenyl derivatives is markedly different from the punctate fluorescence staining of *closo*-1,2-carborane compounds (between **HCPH** and **HCCb**, Fig. 2; **ICPh** and **ICCb**, Supplementary Fig. S1). Such differences had not previously been observed for coumarin dyes functionalised with phenyl or *closo*-1,2-carborane at the 3-position.^[13]

To further confirm the localisation of the probes in cells, co-localisation studies were performed using commercialised

probes that target specific organelles. Co-localisation studies were first conducted against Nile Red, which marks lipid droplets in A549 cells.^[20,21] Lipid droplet homeostasis is critical for cell signalling and the production of

Table 2. HOMO–LUMO energy gaps for the coumarin fluorophores.

Fluorophore	E_{HOMO} (eV)	E_{LUMO} (eV)	ΔE (eV)	λ (nm) ^A
HCPH	-5.5	-2.0	3.5	354
HCoBA	-5.7	-2.1	3.6	344
HCmBA	-5.5	-1.9	3.6	344
HCpBA	-5.4	-1.9	3.5	354
HCCb	-5.6	-1.9	3.7	335
ICPh	-5.4	-2.0	3.4	364
ICCb	-5.8	-2.5	3.3	375

^AWavelength (λ) was calculated using the formula: $\lambda = hc/\Delta E$ (where Planck's constant (h) and speed of light (c)).

inflammatory mediators, with lipid droplet accumulation associated in cancer, cardiovascular diseases and insulin-resistance.^[22] Co-staining studies of the highly lipophilic *ortho*-1,2-carborane derivatives (HCCb and ICCb) with Nile red revealed clear co-localisation (Fig. 3, Pearson's correlation coefficients (PCC) of $R = 0.83 \pm 0.01$ (HCCb) and $R = 0.73 \pm 0.06$ (ICCb)). This indicates a high selectivity for lipid droplets, in comparison to the phenyl derivatives (PCC of $R < 0.5$ for both HCPH and ICPh). The other coumarin probes (HCoBA, HCmBA and HCpBA) did not show lipid droplet staining. Evidently, modifications to the linker group had little effect on the sub-cellular localisation of these probes; it is the terminal EWG that provides the greatest distinction.

Since HCoBA, HCmBA and HCpBA showed punctate staining that was not consistent with the lipid droplets, further co-localisation studies were performed with MitoTracker Red CMXRos and LysoTracker Red DND-99 to probe for mitochondrial or lysosomal localisation, respectively. In neither case was there any significant overlap of the coumarin and the organelle marker. Endoplasmic

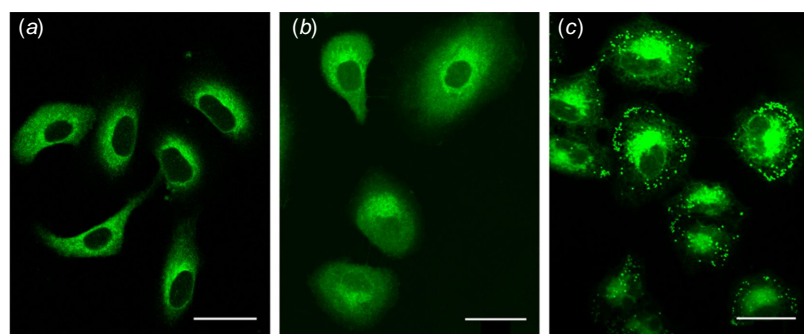


Fig. 2. Confocal microscopy images of A549 cells treated with (a) HCPH (10 μM , 20 min), (b) HCmBA (10 μM , 20 min) and (c) HCCb (10 μM , 20 min), showing coumarin fluorescence ($\lambda_{\text{ex}} = 458$ nm, $\lambda_{\text{em}} = 468$ –568 nm). Scale bar represents 30 μm .

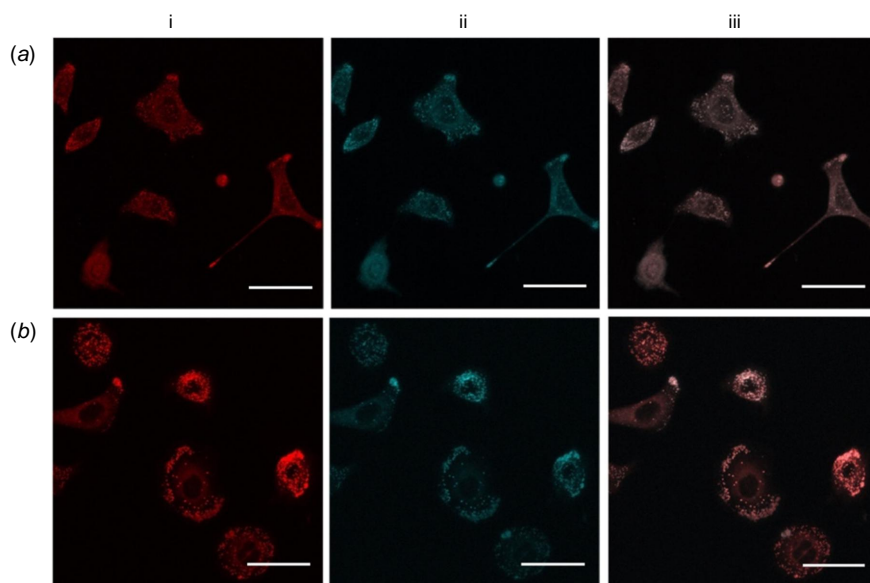


Fig. 3. Confocal microscopy images of A549 cells treated with Nile Red (50 μM , 20 min) and (a) HCCb (10 μM , 20 min) or (b) ICCb (10 μM , 20 min), showing (i) Nile Red fluorescence ($\lambda_{\text{ex}} = 561$ nm, $\lambda_{\text{em}} = 571$ –700 nm), (ii) coumarin fluorescence ($\lambda_{\text{ex}} = 458$ nm, $\lambda_{\text{em}} = 468$ –568 nm) and (iii) overlay of (i) and (ii). Pearson's correlation coefficient for treatment with Nile Red are: HCCb ($R = 0.83 \pm 0.01$) and ICCb ($R = 0.73 \pm 0.06$). Scale bar represents 30 μm .

reticulum (ER) localisation was confirmed by co-staining with an mCherry-ER construct expressed in human colon cancer (DLD-1) cells. While not every cell successfully incorporated the mCherry-ER plasmid, mCherry-stained cells showed colocalisation with **HCoBA**, **HCmBA** and **HCpBA** (PCC of $R = 0.67 \pm 0.03$, 0.60 ± 0.07 and 0.73 ± 0.07 , respectively; Supplementary Fig. S5). No other probes displayed ER localisation. Due to the significance of the ER in numerous pathologies (e.g. neurodegenerative disorders, inflammatory diseases and cancer) for the processing of transmembrane and secreted proteins,^[23] cell-permeable fluorophores, such as **HCoBA**, **HCmBA** or **HCpBA**, could enable the delivery of small molecules to the ER or could prove to be useful small molecule ER markers.

In summary, all probes were observed to be taken up by human cancer cell lines, with significant variations in intracellular localisation owing to modifications in the polarity of the terminal EWG (phenyl, boronic acid and *closo*-carborane functional groups), which may lead to a diverse set of future applications.

Conclusion

Five novel boron-containing coumarin fluorophores (**HCoBA**, **HCmBA**, **HCpBA**, **HCCb** and **ICCb**) were successfully synthesised and characterised in this work. The influence of linker and terminal EWG modifications on the spectroscopic profile of the 7-(diethylamino)-coumarin fluorophore was demonstrated, whereby extension of the π -conjugated bridge at the C3-position provided the greatest overall red-shift. Confocal microscopy studies using A549 lung cancer cells displayed distinctive intracellular localisations of the new coumarin compounds. In particular, the exceptional selectivity of the *closo*-carboranes (**HCCb** and **ICCb**) towards lipid droplets was prevalent compared to their phenyl counterparts (**HCPH** and **ICPH**), and hence these dyes may be adapted for use as a green-emitting alternative to the standard Nile Red (a commonly used lipid-staining dye). Furthermore, the boronic acid fluorophores **HCoBA**, **HCmBA** and **HCpBA** exhibited accumulation in the ER, with potential applications in the design of ER-targeting therapeutics. Structure–photophysical property relationships revealed that the imino-coumarin derivative **ICCb** is an attractive candidate for further development as a NIR coumarin probe, both due to a π -conjugated linker and a strong terminal EWG (*closo*-carborane) that facilitates the ICT process. Ultimately, the incorporation of boron-containing groups into fluorescent scaffolds may prove to be a useful strategy for tuning photophysical and cellular behaviour, with potential developments focussed on boron-based moieties leading to an expansion of exciting new small-molecule tools for biomedical applications.

Experimental

General

All reactions were performed under a nitrogen atmosphere using standard Schlenk technique unless otherwise indicated. All precursor chemicals were commercially available and were purchased from Sigma–Aldrich Co. Anhydrous solvents including acetonitrile, diethyl ether, methanol and dichloromethane were obtained from a solvent purification system, PureSolv MD 7 (Innovative Technology, Inc.). All other solvents were used without any further purification. Column chromatography was carried out using Merck silica gel 60 (230–400 mesh). Analytical thin layer chromatography (TLC) was performed using Merck TLC silica gel 60 F₂₅₄ aluminium plates. Compounds were visualised under shortwave (254 nm) and/or longwave (365 nm) ultraviolet (UV) light. Carborane-containing compounds were visualised on TLC plates using an acidified PdCl₂ (1%) stain and the plates heated by means of a heat gun. Compounds **1–4**, **HCPH** and **ICPH** were synthesised as previously reported.^[7,19,24–27]

Infrared absorption spectra were recorded using a Bruker ALPHA Fourier-transform infrared (FT-IR) spectrometer, with the data reported as wavenumbers (cm⁻¹). All ¹H, ¹¹B{¹H} and ¹³C{¹H} NMR spectra were recorded at 300 K on either a Bruker AVANCE 300 (¹H at 300 MHz, ¹³C at 75 MHz), Bruker AVANCE III 400 (¹H at 400 MHz, ¹¹B at 128 MHz and ¹³C at 100 MHz) or Bruker AVANCE III 500 (¹H at 500 MHz, ¹¹B at 160 MHz and ¹³C at 125 MHz) spectrometer. All NMR signals (δ) are reported in ppm. ¹H and ¹³C NMR spectra recorded using CDCl₃ were referenced to TMS. For all other solvents, the residual solvent peaks were used as internal standards. ¹¹B spectra were referenced automatically by the spectrometer software according to the unified chemical shift scale via the lock frequency of the solvent.^[28] Peak multiplicities have been abbreviated as: s (singlet), d (doublet), dd (doublet of doublets), t (triplet), dt (doublet of triplets), q (quartet), br (broad), and m (multiplet). Low resolution mass spectrometry (LRMS) was performed on a Bruker amazon SL operating in the positive ion mode using electrospray ionisation (ESI) or atmospheric pressure chemical ionisation (APCI). All MALDI mass spectrometric data were obtained using a Bruker Autoflex III matrix assisted laser desorption/ionisation time-of-flight mass spectrometer (MALDI-TOF MS) with delayed extraction using both positive ion and reflector detection modes over the mass range of m/z 300–3000. For the hydrazone-coumarins (**HCoBA**, **HCmBA**, **HCpBA** and **HCCb**), stock solutions of *trans*-2-[3-(4-*tert*-butylphenyl)-2-methyl-2-propenylidene]malononitrile (DCTB) (10 mg mL⁻¹) in 50:50 DCM/MeCN were prepared. The samples were prepared at a concentration of 2 mg mL⁻¹ in DCM. MALDI samples were prepared by combining 20 μ L of matrix solution with 4 μ L of sample solution. A 0.3 μ L portion of this

sample was deposited on a ground steel MALDI target plate and allowed to air dry.

Synthetic procedures

General procedure for the synthesis of the hydrazone-coumarin derivatives (Scheme 1)

A slight excess of a formyl reagent (benzaldehyde, 2-, 3- or 4-formylphenylboronic acid, or **2**) was added to a stirred solution of **1** in absolute ethanol (5 mL). The reaction mixture was heated to reflux. Upon cooling to room temperature, the precipitate was filtered off and washed three times with cold ethanol (3 × 10 mL). NB: Acetonitrile was used as a solvent instead of ethanol in the synthesis of carboranyl hydrazone-coumarin (**HCCb**).

Synthesis of (E)-2-((2-(7-(diethylamino)-2-oxo-2H-chromene-3-carbonyl)hydrazineylidene)methyl)phenyl)boronic acid (HCoBA, Scheme 1)

Formyl reagent: 2-formylphenylboronic acid (103 mg, 0.7 mmol), **1** (100 mg, 0.4 mmol). Reaction time: 18 h. Yield of **HCoBA**: 107 mg (72%) as a dark-yellow crystalline solid. FTIR (cm⁻¹): 3306 (br, OH), 3241 (N–H), 1692 (C=O), 1615 (C=O). δ_{H} (300 MHz, DMSO-*d*₆) 11.71 (s, 1H, NH), 8.74 (s, 1H, H4), 8.68 (s, 1H, H12), 8.48 (s, 2H, B(OH)₂), 7.91 (d, *J* 7.2, 1H, H18), 7.74 (d, *J* 9.0, 1H, H5), 7.68 (d, *J* 3.6, 1H, H15), 7.48–7.37 (m, 2H, H16/17), 6.85 (dd, *J* 11.2, 6.9, 1H, H6), 6.67 (d, *J* 1.9, 1H, H8), 3.51 (q, *J* 6.9, 4H, (CH₃CH₂)₂N–), 1.15 (t, *J* 7.0, 6H, (CH₃CH₂)₂N–). δ_{B} (160 MHz, DMSO-*d*₆) 30.1 (1B). δ_{C} (75 MHz, DMSO-*d*₆) 161.6, 159.2, 157.4, 152.9, 150.0, 148.5, 137.5, 134.6, 131.9, 129.4, 129.0, 126.4, 110.4, 108.7, 108.7, 96.0, 44.5, 12.5. *m/z* (MALDI-TOF MS) calculated for [M + Na]⁺ 430.155, found 430.094.

Synthesis of (E)-3-((2-(7-(diethylamino)-2-oxo-2H-chromene-3-carbonyl)hydrazineylidene)methyl)phenyl)boronic acid (HCmBA, Scheme 1)

Formyl reagent: 3-formylphenylboronic acid (103 mg, 0.7 mmol), **1** (100 mg, 0.4 mmol). Reaction time: 12 h. Yield of **HCmBA**: 129 mg (87%) as a yellow crystalline solid. FTIR (cm⁻¹): 3436 (OH), 3100 (N–H), 1688 (C=O), 1641 (C=O). δ_{H} (400 MHz, DMSO-*d*₆) 11.69 (s, 1H, NH), 8.70 (s, 1H, H4), 8.38 (s, 1H, H12), 8.21 (s, 2H, B(OH)₂), 8.17 (s, 1H, H14), 7.84 (d, *J* 7.3, 1H, H16), 7.75 (d, *J* 7.8, 1H, H18), 7.67 (s, *J* 9.0, 1H, H5), 7.42 (t, *J* 7.5, 1H, H17), 6.75 (dd, *J* 9.0, 2.0, 1H, H6), 6.57 (d, *J* 1.9, 1H, H8), 3.43 (q, *J* 7.0, 4H, (CH₃CH₂)₂N–), 1.11 (t, *J* 7.0, 6H, (CH₃CH₂)₂N–). δ_{B} (160 MHz, DMSO-*d*₆) 28.6 (1B). δ_{C} (75 MHz, DMSO-*d*₆) 161.5, 159.0, 157.3, 152.7, 148.6, 148.4, 135.8, 133.2, 132.8, 131.8, 129.1, 127.8, 110.3, 108.6, 107.9, 95.9, 44.4, 12.3. *m/z* (MALDI-TOF MS) calc. for [M + H]⁺ 408.173, found 408.200.

Synthesis of (E)-4-((2-(7-(diethylamino)-2-oxo-2H-chromene-3-carbonyl)hydrazineylidene)methyl)phenyl)boronic acid (HCpBA, Scheme 1)

Formyl reagent: 4-formylphenylboronic acid (103 mg, 0.7 mmol), **1** (100 mg, 0.4 mmol). Reaction time: 8 h. Yield of **HCpBA**: 145 mg (98%) as a yellow crystalline solid. FTIR (cm⁻¹): 3306 (br, OH), 3118 (N–H), 1702 (C=O), 1667 (C=O). δ_{H} (400 MHz, DMSO-*d*₆) 11.74 (s, 1H, NH), 8.76 (s, 1H, H4), 8.43 (s, 1H, H12), 8.13 (s, 2H, B(OH)₂), 7.86 (d, *J* 8.0, 2H, H15), 7.74 (d, *J* 9.1, 1H, H5), 7.70 (d, *J* 8.1, 2H, H14), 6.84 (dd, *J* 11.3, 6.8, 1H, H6), 6.66 (d, *J* 2.0, 1H, H8), 3.50 (q, *J* 7.0, 4H, (CH₃CH₂)₂N–), 1.15 (t, *J* 7.0, 6H, (CH₃CH₂)₂N–). δ_{B} (160 MHz, DMSO-*d*₆) 31.7 (1B). δ_{C} (75 MHz, DMSO-*d*₆) 161.5, 159.0, 157.4, 152.8, 148.5, 148.3, 135.6, 134.4, 131.8, 126.1, 110.4, 108.5, 107.9, 95.9, 44.4, 12.29. *m/z* (MALDI-TOF MS) calc. for [M + H]⁺ 408.173, found 408.210.

Synthesis of 7-(diethylamino)-2-oxo-3-((closo-1,2-carboranyl)carbohydrazide)-2H-chromene-2-one (HCCb, Scheme 1)

Formyl reagent: **2** (17 mg, 0.1 mmol), **1** (13.6 mg, 0.5 mmol). Yield of **HCCb**: 9.34 mg (44%) as an orange crystalline solid. FTIR (cm⁻¹): 3371 (N–H), 2529 (BH), 1680 (C=O), 1649 (C=O). δ_{H} (400 MHz, DMSO-*d*₆) 11.82 (s, 1H, NH), 8.71 (s, 1H, H4), 8.17 (s, 1H, H12), 7.74 (d, *J* 9.0, 1H, H5), 6.85 (d, *J* 9.1, 1H, H6), 6.65 (d, *J* 1.6, 1H, H8), 5.38 (br s, 1H, H14), 3.51 (q, *J* 7.0, 4H, (CH₃CH₂)₂N–), 3.45–1.20 (br, B–H, 10H), 1.15 (t, *J* 7.0, 6H, (CH₃CH₂)₂N–). δ_{B} (128 MHz, DMSO-*d*₆) –3.1 (2B), –9.6 (4B), –11.9 (4B). δ_{C} (75 MHz, CDCl₃) 162.8, 160.6, 158.2, 153.4, 149.6, 141.1, 131.7, 110.5, 108.5, 107.8, 96.6, 77.4, 57.1, 45.3, 12.4. *m/z* (MALDI-TOF MS) calc. for [M + H]⁺ 430.313, found 430.451.

Synthesis of (E)-7-(diethylamino)-3-((closo-1,2-carboranylimino)methyl)-2H-chromen-2-one (ICCb, Scheme 2)

Compound **ICCb** was prepared by refluxing **4** (20 mg, 0.1 mmol) with **3** (61.6 mg, 0.3 mmol) in MeCN for 14 h. Purification was achieved by means of preparative TLC (DCM/hexane, 70:30) to afford **ICCb** (22 mg, 57%), as an orange crystalline solid. FTIR (cm⁻¹): 2574 (BH), 1707 (C=N), 1620 (C=O). δ_{H} (400 MHz, CDCl₃) 8.59 (s, 1H, H11), 8.20 (s, 1H, H4), 7.34 (d, *J* 9.0, 1H, H5), 6.62 (dd, *J* 11.4, 6.6, 1H, H6), 6.48 (d, *J* 2.2, 1H, H8), 4.03 (br s, 1H, H13), 3.46 (q, *J* 7.1, 4H, (CH₃CH₂)₂N–), 3.45–1.20 (br, 10H, B–H), 1.25 (t, *J* 7.1, 6H, (CH₃CH₂)₂N–). δ_{B} (128 MHz, CDCl₃) –3.71 (2B), –8.09 (2B), –10.23 (2B), –12.13 (2B), –14.04 (2B). δ_{C} (75 MHz, CDCl₃) 161.8, 158.4, 153.1, 142.9, 131.6, 112.7, 110.2, 108.6, 97.3, 94.0, 77.4, 62.1, 45.3, 12.6. *m/z* (APCI MS) calc. for [M + H]⁺ 388.28, found 388.28.

Table 3. Probes or plasmid used to assess for co-localisation against various sub-cellular compartments.

Probe or plasmid	Sub-cellular compartment assessed for co-localisation	Emission range acquired on the Leica SP5 (nm)
Nile Red (50 μ M)	Lipid droplets	571–700
MitoTracker Red CMXRos (100 nM)	Mitochondria	570–767
LysoTracker Red DND-99 (50 nM)	Lysosomes	568–701
mCherry-ER construct	Endoplasmic reticulum	581–653

Fluorescence spectroscopy

All fluorescence studies were performed in absolute ethanol at a concentration of 1 μ M, measured on a Varian Cary Eclipse fluorescence spectrophotometer using 1 cm path-length quartz cuvettes.

Quantum yields were measured and calculated using a PTI QuantaMaster 400 spectrofluorometer with an integrating sphere (IS) detector, using the absolute quantum yield method. These measurements were performed at room temperature with dilute fluorophore samples (conc. < 1 μ M). Excitation and emission correction were performed by the instrument.

Mammalian cell studies

Human cell lines

Human alveolar adenocarcinoma (A549) cells were used in this study. Cells were cultured at 37°C with 5% CO₂ as monolayers in exponential growth. Cells were maintained in Advanced Dulbecco's Modified Eagle Medium (ADMEM) supplemented with 2% foetal bovine serum (FBS) and 2 mM glutamine. Subculturing of cells were performed every 3–4 days when 80% confluency was reached. Trypsin–EDTA (0.25%) were used to facilitate dislodgement of cells from the flask during sub-culturing.

For determining co-localisation with ER, human colorectal adenocarcinoma (DLD-1) cells, previously transfected with a mCherry fluorescent protein tagged to the ER, were used. Cells were cultured at 37°C with 5% CO₂ as monolayers at exponential growth. Cells were maintained in ADMEM supplemented with 2% FBS, 400 μ g mL⁻¹ gentamycin and 2 mM glutamine. Subculturing of cells were performed every 3–4 days when 80% confluency was reached. Trypsin–EDTA (0.25%) was used to facilitate dislodgement of cells from the flask during sub-culturing.

Confocal microscopy imaging

Approximately 100 000 cells were seeded on 35 mm MatTek dishes pre-coated with L-proline and allowed to adhere overnight. Cells were then dosed with a 10 μ M coumarin compound in DMSO (final DMSO concentration < 1% (v/v)) in ADMEM (supplemented with 2% FBS, 2 mM glutamine) for

20 min at 37°C. Cells were then imaged in FluoroBrite DMEM media (1 mL, supplemented with 10% FBS, 2 mM glutamine).

Fluorescent micrographs were acquired using an Olympus Fluoview FV1000 inverted microscope equipped with a UPLSAPO 60X water-immersion objective lens (N.A. = 1.15). Coumarin probes were excited at 458 nm using an Argon laser, and fluorescence emitted between 468 and 568 nm was acquired. Fluorescent images were collected using FV10-ASW viewer software v1.7 (Olympus) and processed using Image J[®] (Fig. 2, Supplementary Fig. S1).

Co-localisation studies with commercial fluorescent probes

For assessing co-localisation of probes in the various organelles, A549 cells were incubated concurrently with 10 μ M coumarin dye and respective commercial fluorescent probes (Table 3) in ADMEM (supplemented with 2% FBS, 2 mM glutamine) for 20 min at 37°C. Excess probes were washed and imaged in FluoroBrite DMEM media (1 mL, supplemented with 10% FBS, 2 mM glutamine).

Co-localisation studies were performed using a Leica SP5 microscope equipped with a 63.0 \times (N.A. = 1.20) water-immersion objective lens. Fluorescence emitted from the coumarin probes was collected between 468 and 568 nm (458 nm laser excitation). Fluorescence from the respective sub-cellular localising commercial probes or plasmid are listed in Table 3, a 561 nm laser excitation was used. Images acquired were processed on Image J[®]. Co-localisation assessments were performed using the Coloc 2 plugin determined by the Pearson's correlation coefficient. A *R*-value of less than 0.5 indicates no co-localisation, while a *R*-value of more than 0.7 is interpreted as co-localisation with the organelle assessed.^[29,30]

Supplementary material

Supplementary figures, including additional confocal microscopy images, fluorescence, NMR and MS spectra are available [online](#).

References

- [1] Jonkman J, Brown CM. *J Biomol Tech* 2015; 26: 54–65. doi:10.7171/jbt.15-2602-003

- [2] Vahrmeijer AL, Hutteman M, van der Vorst JR, van de Velde CJH, Frangioni J V. *Nat Rev Clin Oncol* 2013; 10: 507–18. doi:10.1038/nrclinonc.2013.123
- [3] Gibbs SL. *Quant Imaging Med Surg* 2012; 2: 177–87.
- [4] Boni L, David G, Mangano A, Dionigi G, Rausei S, Spampatti S. *Surg Endosc* 2015; 29: 2046–55. doi:10.1007/s00464-014-3895-x
- [5] Qin J, Yang Z. *Anal Methods* 2015; 7: 2036–40. doi:10.1039/C4AY02971B
- [6] He S, Song J, Qu J, Cheng Z. *Chem Soc Rev* 2018; 47: 4258–78. doi:10.1039/C8CS00234G
- [7] Niu G, Liu W, Xiao H, Zhang H, Chen J, Dai Q. *Chem Asian J* 2016; 11: 498–504. doi:10.1002/asia.201501026
- [8] Chen J, Liu W, Zhou B, Niu G, Zhang H, Wu J. *J Org Chem* 2013; 78: 6121–30. doi:10.1021/jo400783x
- [9] Liu X, Cole JM, Waddell PG, Lin TC, Radia J, Zeidler A. *J Phys Chem A* 2012; 116: 727–37. doi:10.1021/jp209925y
- [10] Musa M, Cooperwood J, Khan MO. *Curr Med Chem* 2008; 15: 2664–79. doi:10.2174/092986708786242877
- [11] Nagasawa Y, Yartsev AP, Tominaga K, Johnson AE, Yoshihara K. *J Am Chem Soc* 1993; 115: 7922–3. doi:10.1021/ja00070a066
- [12] DiCesare N, Lakowicz JR. *J Biomed Opt* 2002; 7: 538–45. doi:10.1117/1.1502263
- [13] Wu A, Kolanowski JL, Boumelhem BB, Yang K, Lee R, Kaur A. *Chem Asian J* 2017; 12: 1704–8. doi:10.1002/asia.201700423
- [14] Guo Z, Shin I, Yoon J. *ChemComm* 2012; 48: 5956–67. doi:10.1039/c2cc31985c
- [15] Issa F, Kassiou M, Rendina LM. *Chem Rev* 2011; 111: 5701–22. doi:10.1021/cr2000866
- [16] Kahlert J, Austin CJD, Kassiou M, Rendina LM. *Aust J Chem* 2013; 66: 1118–23. doi:10.1071/CH13256
- [17] Kahlert J, Böhling L, Brockhinke A, Stammler H-G, Neumann B, Rendina LM. *Dalton Trans* 2015; 44: 9766–81. doi:10.1039/C5DT00758E
- [18] Ma Y, Luo W, Quinn PJ, Liu Z, Hider RC. *J Med Chem* 2004; 47: 6349–62. doi:10.1021/jm049751s
- [19] Takechi H, Oda Y, Nishizono N, Oda K, Machida M. *Chem Pharm Bull* 2000; 48: 1702–10. doi:10.1248/cpb.48.1702
- [20] Chowdhury R, Jana B, Saha A, Ghosh S, Bhattacharyya K. *Medchemcomm* 2014; 5: 536–39. doi:10.1039/c3md00269a
- [21] Boumelhem BB, Pilgrim C, Zwicker VE, Kolanowski JL, Yeo JH, Jolliffe KA. *J Cell Sci* 2022; 135: jcs258322. doi:10.1242/jcs.258322
- [22] Cruz ALS, Barreto E, de A, Fazolini NPB, Viola JPB, Bozza PT. *Cell Death Dis* 2020; 11: 105. doi:10.1038/s41419-020-2297-3
- [23] Li A, Song N-J, Riesenberger BP, Li Z. *Front Immunol* 2020; 10: 1–15. doi:10.3389/fimmu.2019.03154
- [24] Dozzo P, Kasar RA, Kahl SB. *Inorg Chem* 2005; 44: 8053–7. doi:10.1021/ic0506660
- [25] Wu J-S, Liu W-M, Zhuang X-Q, Wang F, Wang P-F, Tao S-L. *Org Lett* 2007; 9: 33–6. doi:10.1021/ol062518z
- [26] Zhou Z, Li N, Tong A. *Anal Chim Acta* 2011; 702: 81–6. doi:10.1016/j.aca.2011.06.041
- [27] Nie Y, Wang Y, Miao J, Li Y, Zhang Z. *J Organomet Chem* 2015; 798: 182–8. doi:10.1016/j.jorganchem.2015.05.046
- [28] Antoniadou MA, Eleftheriades G V. *Proc 5th Eur Conf Antennas Propagation, EUCAP 2011* 2011; 73: 2406–9.
- [29] Bolte S, Cordelières FP. *J Microsc* 2006; 224: 213–32. doi:10.1111/j.1365-2818.2006.01706.x
- [30] Aaron JS, Taylor AB, Chew T-L. *J Cell Sci* 2018; 131: jcs211847. doi:10.1242/jcs.211847

Data availability. The data that support this study are available in the article and accompanying online supplementary material.

Conflicts of interest. The authors declare no conflicts of interest.

Declaration of funding. A. M. and K. G. L. acknowledge the Australian Government for a Research Training Program Scholarship. L.M.R. is grateful for past and present funding from the Australian Research Council, Cure Cancer Foundation of Australia, National Breast Cancer Foundation, and the Prostate Cancer Foundation of Australia. E. J. N. acknowledges the Australian Research Council (DPI180101353, DPI180101897, CE200100012) for funding.

Acknowledgements. The authors acknowledge the support of the facilities and the scientific and technical assistance provided by the Australian Microscopy and Microanalysis Research Facility at the Australian Centre for Microscopy and Microanalysis (ACMM) at the University of Sydney, and thank Dr Samrat Dasgupta for providing the 1-amino-ortho-carborane derivative (4). This research was facilitated by access to Sydney Analytical, a core research facility at the University of Sydney.

Author affiliations

^ASchool of Chemistry, The University of Sydney, Sydney, NSW 2006, Australia.

^BThe University of Sydney Nano Institute, Sydney, NSW 2006, Australia.

^CAustralian Research Council Centre of Excellence for Innovations in Peptide and Protein Science, The University of Sydney, Sydney, NSW 2006, Australia.